

AFRL-AFOSR-UK-TR-2011-0020



Nonlinear Dynamics of Globally Coupled Sine-Gordon Equations

Boris A. Malomed

**Tel Aviv University
Department of Physical Electronics
Faculty of Engineering
Tel Aviv, Israel 69978**

EOARD GRANT 09-3034

May 2011

Final Report for 18 August 2009 to 18 August 2010

Distribution Statement A: Approved for public release distribution is unlimited.

**Air Force Research Laboratory
Air Force Office of Scientific Research
European Office of Aerospace Research and Development
Unit 4515 Box 14, APO AE 09421**

REPORT DOCUMENTATION PAGE

Form Approved OMB No. 0704-0188

Public reporting burden for this collection of information is estimated to average 1 hour per response, including the time for reviewing instructions, searching existing data sources, gathering and maintaining the data needed, and completing and reviewing the collection of information. Send comments regarding this burden estimate or any other aspect of this collection of information, including suggestions for reducing the burden, to Department of Defense, Washington Headquarters Services, Directorate for Information Operations and Reports (0704-0188), 1215 Jefferson Davis Highway, Suite 1204, Arlington, VA 22202-4302. Respondents should be aware that notwithstanding any other provision of law, no person shall be subject to any penalty for failing to comply with a collection of information if it does not display a currently valid OMB control number.
PLEASE DO NOT RETURN YOUR FORM TO THE ABOVE ADDRESS.

| | | |
|--|---------------------------------------|--|
| 1. REPORT DATE (DD-MM-YYYY) 16-05-2011 | 2. REPORT TYPE Final Report | 3. DATES COVERED (From - To) 18 August 2009 - 18 August 2010 |
|--|---------------------------------------|--|

| | |
|--|--|
| 4. TITLE AND SUBTITLE Nonlinear Dynamics of Globally Coupled Sine-Gordon Equations | 5a. CONTRACT NUMBER FA8655-09-1-3034 |
| | 5b. GRANT NUMBER Grant 09-3034 |
| | 5c. PROGRAM ELEMENT NUMBER 61102F |

| | |
|---|-----------------------------|
| 6. AUTHOR(S) Professor Boris A. Malomed | 5d. PROJECT NUMBER |
| | 5d. TASK NUMBER |
| | 5e. WORK UNIT NUMBER |

| | |
|--|--|
| 7. PERFORMING ORGANIZATION NAME(S) AND ADDRESS(ES) Tel Aviv University Department of Physical Electronics Faculty of Engineering Tel Aviv, Israel 69978 | 8. PERFORMING ORGANIZATION REPORT NUMBER N/A |
|--|--|

| | |
|---|---|
| 9. SPONSORING/MONITORING AGENCY NAME(S) AND ADDRESS(ES) EOARD Unit 4515 BOX 14 APO AE 09421 | 10. SPONSOR/MONITOR'S ACRONYM(S) AFRL/AFOSR/RSW (EOARD) |
| | 11. SPONSOR/MONITOR'S REPORT NUMBER(S) AFRL-AFOSR-UK-TR-2011-0020 |

12. DISTRIBUTION/AVAILABILITY STATEMENT
Approved for public release; distribution is unlimited.

13. SUPPLEMENTARY NOTES

14. ABSTRACT

This paper reports results of the systematic analysis of the dynamics of fluxons (kinks) in the fundamental prismatic configuration formed by three bulk superconductors, which creates a set of three parallel long Josephson junctions at interfaces between them. The setting is described by a system of three coupled sine-Gordon equations for the phases corresponding to each junction. In fact, the condition for the external magnetic flux trapped by the system reduces the model to two equations. The equations include the dissipative terms, and are controlled by the frustration parameter, that measures the deviation of the external flux from half a quantum. Analyzing the corresponding potential profile, we have identified different types of topological kink solitons, which correspond to fluxons, in terms of the coupled junctions. Nontopological "bubble" modes have been found too. Some solutions, including those for "compound" kinks and for two types of the bubbles, were obtained in an analytical form. Numerical simulations demonstrate that the compound kinks are unstable against breaking up into pairs of simple kinks. Bubbles are metastable objects, that eventually break up into kink-antikink pairs. The system also gives rise to kinks which connect different potential minima, hence they are pulled by the tilt of the potential. Using the momentum-balance method, we have derived the equilibrium velocity at which such driven kinks should move, and verified the prediction by simulations. Finally, collisions between the moving kinks were studied by means of direct simulations, which demonstrate that the collisions are always strongly inelastic.

15. SUBJECT TERMS
EOARD, Superconductivity

| | | | | | |
|--|------------------------------|-------------------------------|--|--------------------------------------|--|
| 16. SECURITY CLASSIFICATION OF: | | | 17. LIMITATION OF ABSTRACT SAR | 18. NUMBER OF PAGES 27 | 19a. NAME OF RESPONSIBLE PERSON SCOTT DUDLEY, Lt Col, USAF |
| a. REPORT UNCLAS | b. ABSTRACT UNCLAS | c. THIS PAGE UNCLAS | | | 19b. TELEPHONE NUMBER (Include area code) +44 (0)1895 616162 |

**Report from Boris Malomed to the European Office of
Aerospace Research and Development (EOARD)
Project: "Nonlinear Dynamics of Globally Coupled Sine
Gordon Equations",
Award no. FA8655-09-1-3034**

Title of the paper summarizing the results:
Fluxons in a triangular set of coupled Josephson junctions

Boris A. Malomed

Department of Physical Electronics, School of Electrical Engineering, Faculty of Engineering,
Tel Aviv University, Tel Aviv 69978, Israel

Abstract

We report results of the analysis of dynamics of fluxons (topological solitons, alias kinks) in the system of three long Josephson junctions between three bulk superconductors which form a prism. The system is modeled by coupled sine-Gordon equations for phases of the junctions. The relation for the flux trapped inside the prism reduces the system from three equations to two. They include dissipative terms, and are controlled by the frustration parameter, which measures the deviation of the trapped flux from half a quantum. Analyzing the effective potential of the coupled equations, we identify different species of kinks and nontopological "bubble" modes in this system. Solutions for compound kinks and for two types of the bubbles are obtained in an explicit analytical form. Numerical tests demonstrate that the compound kinks are unstable against breakup into pairs of separating simple kinks. The bubbles feature metastability, eventually breaking up into kink-antikink pairs. Kinks which connect different potential minima and are, accordingly, pulled by the potential difference, are considered too. Using the momentum-balance method, we predict the velocity at which these kinks should move in the presence of the dissipation, Numerical tests demonstrate that the analysis predicts the velocity in a virtually exact form. Inelastic collisions between the moving kinks are studied too.

The work has been conducted in close collaboration with Dr. Stanford Yukon of Division of Electromagnetic Technologies, USAF Research Laboratory, Hanscom AFB, MA 01731, USA. In particular, I was responsible for the analytical part of the work, while numerical calculations have been chiefly carried out by Dr. Yukon. The following text is a preprint of a paper summarizing results produced by the work on this project. The paper, to be co-authored by S. Yukon and B. A. Malomed, will be submitted to Phys. Rev. B.

PACS numbers: 74.81.Fa; 74.50.+k; 03.75.Lm; 05.45.Yv

1. Introduction

The dynamics of topological phase solitons, which represent quanta of the magnetic flux, i.e., *fluxons*, in long Josephson junctions (thin dielectric layers separating two bulk superconductors) has been a subject of many experimental and theoretical works published in the course of more than 30 last years – see, e.g., original papers [1-5] and reviews [6,7]. A fundamental model of the fluxon dynamics is based on the sine-Gordon equation with additional terms which account for various physical effects, such as dissipation and driving fields [1,5]. Similar extended versions of the sine-Gordon equations apply to the description of a number of other physical media, such as charge-density waves in chain conductors, dislocations in crystals, etc. [6,8]. In the field of the Josephson physics, a great deal of attention was attracted to the study of diverse aspects of the fluxon dynamics in *coupled* parallel junctions [4]. In particular, shuttle oscillations of many-fluxon complexes may find an important application to the generation of coherent THz radiation [9]. Commonly adopted models for coupled junctions are based on systems of sine-Gordon equations coupled by terms which account for the magnetic interactions between parallel layers [4,6,7,9].

Most works dealing with fluxons in coupled junctions considered pairs of parallel junctions or multi-layer stacks [4,9]. Another fundamentally interesting configuration is the one in which three bulk superconductors are put together to build a prism, which gives rise to a symmetric triangular set of three Josephson junctions emerging at interfaces between the superconductors [5,10]. An essential peculiarity of this setting is that the prismatic structure may trap magnetic flux, which strongly affects the dynamics of phase solitons in the triangular Josephson set. The dynamics features a degeneracy when the trapped flux is exactly equal to half a quantum. Then, a small deviation of the trapped flux from this special value plays the role of frustration which lifts the degeneracy.

It is relevant to mention that symmetric triangular sets of coupled nonlinear dynamical elements occur in other areas, where specific features of symmetric and broken-symmetry states in such setting have been studied in some detail. These systems include sets of three effective potential wells for light beams in photonic media [11], Bose-Hubbard systems with three sites [12], quantum phase transitions and Josephson oscillations in sets of three coupled potential wells [13], and nonlocal interactions in dipolar Bose-Einstein condensates (BECs) loaded into a set of three potential wells [14]. Symmetric and asymmetric states of interacting solitons in three-core systems were studied too, including a triangular configuration of linearly coupled parallel fiber Bragg gratings [15], coupled triplets of Gross-Pitaevskii equations with applications to the description of three-component BEC [16], and dissipative solitons, including vortices, in a symmetric system of three linearly-coupled complex Ginzburg-Landau equations [17].

Our objective in this work is to develop a systematic analysis of the phase-soliton dynamics in the system of three coupled long Josephson junctions, using the model

Nonlinear Dynamics of Globally Coupled Sine Gordon Equations

derived in Ref. [5]. In Section 2, we start by introducing the model (due to the constraint imposed by the trapped magnetic flux, the respective system of three coupled sine-Gordon equations is reduced to two) and analyzing various types of static kinks, which may exist in this system as stationary solutions connecting local minima or saddle points of the corresponding effective potential in the plane of two phase variables. The static kinks (fluxons) of two essentially different types are possible in the system, "simple" and "compound" ones, which correspond, respectively, to the 2π steps in one or both independent phases. A solution for the compound kink is found in an explicit analytical form for arbitrary values of frustration parameter. Further, direct simulations demonstrate that the compound fluxons are unstable: the evolution leads to their spontaneous breakup into a pair of separating simple fluxons, while the simple fluxons themselves are completely stable topological solitons. The possibility of the splitting of the compound kink into the pair of simple ones can be readily explained by comparison of their energies.

The structure of the model also admits solutions of another type, in the form of "bubbles", i.e., soliton-like modes built on top of a constant background, with zero topological charge. Two analytical solutions for the bubbles are found in Section 3. The simulations demonstrate that the bubbles are metastable modes, which persist for a relatively long time, but eventually break up into pairs of separating kinks.

The same system gives rise to kinks of a different type, which connect backgrounds with different energy densities, which correspond to deeper and shallower potential minima, alias a "true vacuum" and a "false" one. In the conservative system, the potential tilt makes the existence of such kinks in a steady state impossible. However, in the presence of the dissipation terms, the balance of the driving potential force and dissipation-induced friction creates kinks (alias shock waves, in this context) traveling at the corresponding equilibrium velocity. In Section 4, we find this velocity in an analytical form, using the momentum-balance analysis [1,5]. The result is found to be in a practically exact agreement with numerical findings (and the traveling kinks are found to be completely stable). Continuing the work with the moving kinks, in Section 5 we study collisions between them, by means of direct simulations, which demonstrate that the collisions are strongly inelastic; in particular, some colliding pairs annihilate into persistent quiescent breathers. The work is concluded by Section 6.

2. Kinks connecting true vacuums

The system that we investigate here is formed by coupling three long Josephson junctions such that each one shares a common superconductor with its two neighbors. In the usual notation, the generalized sine-Gordon equations for the phases of the three junctions (jumps of the phases of the wave function of superconducting electrons across each junction), including the Ohmic losses with coefficient α , can be written as [5,10]

Nonlinear Dynamics of Globally Coupled Sine Gordon Equations

$$\begin{aligned} (\phi_1)_{tt} - (\phi_1)_{xx} + \alpha (\phi_1)_t + \frac{2}{1+2\eta} \sin \phi_1 + \frac{1}{1+2\eta} [\sin \phi_2 + \sin(\phi_1 - \phi_2 + \delta)] &= 0, \\ (\phi_2)_{tt} - (\phi_2)_{xx} + \alpha (\phi_2)_t + \frac{2}{1+2\eta} \sin \phi_2 + \frac{1}{1+2\eta} [\sin \phi_1 - \sin(\phi_1 - \phi_2 + \delta)] &= 0, \end{aligned} \quad (1)$$

where it is assumed that the ratio of the capacitance per unit length of the third junction to that of the other two junctions is η , and, simultaneously, the same ratio for the inductance per unit length is $1/\eta$ (these assumptions make it possible to account for the possible difference in characteristics of the three junctions, while keeping equal Swihart velocities in them). System (1) contains only two equations, because, in the limit of zero transverse inductance, the phase of the third junction is determined by the constraint imposed by external flux Φ trapped in the system, $\phi_3 = \phi_1 - \phi_2 - \phi$, where $\phi = 2\pi\Phi / \Phi_0 \equiv \pi + \delta$ is the phase corresponding to the external flux, Φ_0 is the flux quantum, and parameter δ , which accounts for the deviation of the trapped flux from half the quantum, determines the system's *frustration*.

The energy conserved by system (1) in the absence of the dissipative terms ($\alpha = 0$) is

$$\begin{aligned} E = \int_{-\infty}^{+\infty} \left\{ \frac{1}{2} \left[(\phi_1)_t^2 + (\phi_2)_t^2 + \eta \left((\phi_1)_t - (\phi_2)_t \right)^2 + (\phi_1)_x^2 + (\phi_2)_x^2 + \eta \left((\phi_1)_x - (\phi_2)_x \right)^2 \right] \right. \\ \left. - \cos \phi_1 - \cos \phi_2 + \cos(\phi_1 - \phi_2 - \delta) - \mathbf{C}(\infty) \right\} dx, \end{aligned} \quad (2)$$

where $\mathbf{C}(\infty)$ stands for the value of the combination of the three cosines at $x = \pm\infty$ (the subtraction of this constant terms secures the convergence of the integrated energy [10]). Below, we will also need an expression for the momentum of system (1), which is also conserved if $\alpha = 0$:

$$\begin{aligned} P &= - \int_{-\infty}^{+\infty} \left[(\phi_1)_x (\phi_1)_t + (\phi_2)_x (\phi_2)_t + \eta (\phi_3)_x (\phi_3)_t \right] dx \\ &\equiv - \int_{-\infty}^{+\infty} \left[(1+\eta) (\phi_1)_x (\phi_1)_t + (1+\eta) (\phi_2)_x (\phi_2)_t - \eta (\phi_1)_x (\phi_2)_t - \eta (\phi_2)_x (\phi_1)_t \right] dx. \end{aligned} \quad (3)$$

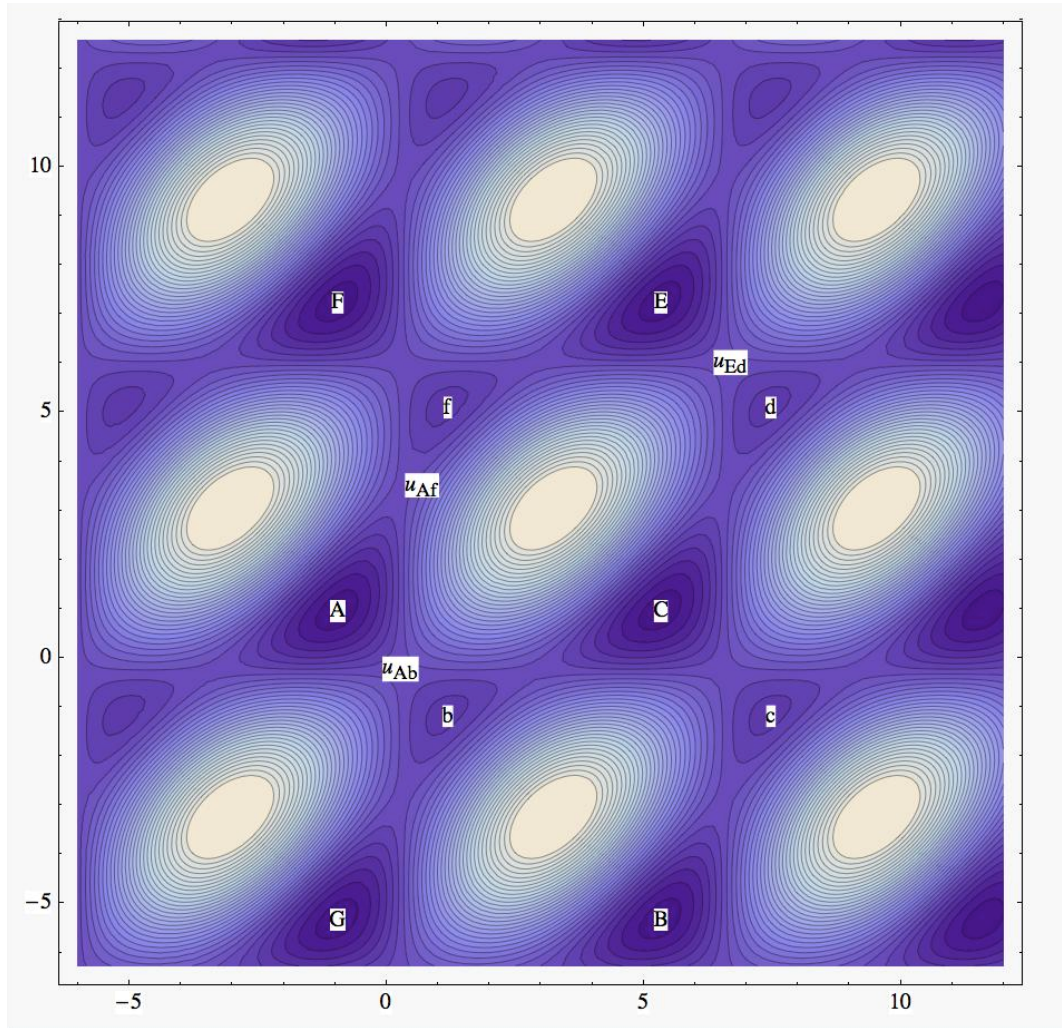
The potential part of energy (2) is

$$V(\phi_1, \phi_2) = -\cos \phi_1 - \cos \phi_2 - \cos(\phi_1 - \phi_2 - \phi), \quad (4)$$

which is plotted, in the plane of (ϕ_1, ϕ_2) , in Fig. 1 for frustration $\delta = 0.1\pi$. When $\delta = 0$, all local minima of the potential have equal depths, and thus represent "true vacuums" of the system. In this case, the stationary version of Eqs. (4) gives rise to kink solutions that connect these minima. The kinks at $\delta = 0$ feature the fractional flux content, that appears in multiples of $\Phi_0/3$ [5]. When $\delta \neq 0$, the potential minima that are labeled {A,

Nonlinear Dynamics of Globally Coupled Sine Gordon Equations

B, G} in Fig. 1 are the true (lowest-energy) vacuum states, while shallower minima, with a higher potential energy, that are labeled {a, b, g}, may be called "false vacuum states". Symbols μ in Fig. 1 mark saddle points of the potential.



(Color online) Fig. 1. Contour plots of potential function (4) with labeled minima and saddle points, for $\delta = 0.1\pi$.

The values of the coordinates at minima and saddle points of potential $V(\phi_1, \phi_2)$, (ϕ_1^*, ϕ_2^*) , are found from equations $\partial V / \partial \phi_{1,2} = 0$, i.e.,

$$\begin{aligned} \sin(\phi_1^*) - \sin(\phi_1^* - \phi_2^* - \delta) &= 0, \\ \sin(\phi_2^*) + \sin(\phi_1^* - \phi_2^* - \delta) &= 0, \end{aligned} \tag{5}$$

which yields

Nonlinear Dynamics of Globally Coupled Sine Gordon Equations

$$\begin{aligned}\phi_1^* &= (1/3)[(\pi + \delta) + 2\pi(n + 2m)], \\ \phi_2^* &= (1/3)[-(\pi + \delta) + 2\pi(n + 1)],\end{aligned}\tag{6}$$

where n and m are arbitrary integers. In particular, for $\delta = \pi/10$ Eqs. (6) give rise to the grid of minimum points displayed in Fig. 1, namely, point A for $m = 1, n = 0$:

$$(\phi_1^*, \phi_2^*) = \frac{1}{3}(-\pi + \delta, \pi - \delta) \rightarrow (-0.942, 0.942),\tag{7}$$

and point b for $m = n = 0$:

$$(\phi_1^*, \phi_2^*) = \frac{1}{3}(\pi + \delta, -\pi - \delta) \rightarrow (-1.151, 1.151).\tag{8}$$

All other minima may be found by adding or subtracting multiples of 2π to points (7) and (8). Further, the saddle point u_{Ab} marked in Fig. 1 has coordinates $(\phi_1^*, \phi_2^*) = (\delta, -\delta)$, from which all other saddle points can be obtained by adding or subtracting multiples of 2π .

Static kink solutions connect adjacent minima of the potential with equal depths, shifted by 2π in either or both directions (for instance, simple kinks may connect points A and C or C and B in Fig. 1, while a "compound" kink links points A and B in the diagonal direction). For these solutions, the stationary version of Eqs. (1) reduces to the equations of motion for a test particle with two degrees of freedom, (ϕ_1, ϕ_2) and unit mass, in the pseudo-potential $U(\phi_1, \phi_2) \equiv -V(\phi_1, \phi_2)$, with coordinate x playing the role of time. In the rest of the paper, we focus on the most fundamental case of $\eta = 1$ in Eqs. (1).

For the "compound" kink solution connecting points A and B, and passing through saddle point u_{Ab} and the shallower minimum b, one can set $\phi_1 = \phi_2$. After simple manipulations with the resulting mechanical equation for the single remaining degree of freedom, the kink solution, $\phi(x)$, can be found in an explicit form:

$$\phi_{AB}(x, \delta) = 2 \tan^{-1} \left\{ \frac{4a_r c_r^2 e^{\alpha x / \sqrt{3}} - 4\alpha(|c|^2 - a_r c_r) e^{\alpha x / 2\sqrt{3}} - a_r \alpha^2}{\left[2\alpha(a_r - c_r + \alpha) e^{\alpha x / 2\sqrt{3}} - \alpha \right] \left[2\alpha(a_r - c_r - \alpha) e^{\alpha x / \sqrt{3}} - \alpha \right]} \right\}.\tag{9}$$

The constants here are defined via roots $t_{1,2,3,4}$ of the quartic polynomial which emerges in the course of the integration of the equation for the kink's shape,

$$a_0 + a_1 t + a_2 t^2 + a_3 t^3 + a_4 t^4 = 0,\tag{10}$$

Nonlinear Dynamics of Globally Coupled Sine Gordon Equations

with $t \equiv \tan(\phi_1/2)$, and the coefficients determined by values of frustration δ and effective energy, $E \equiv 6U(\phi_1) \equiv 2\cos\phi_1 - \cos(2\phi_1 - \delta)$, taken at the points connected by the kink solution:

$$\begin{aligned} a_0 &= E - 2 + \cos\delta, \\ a_1 &= 4\cos\delta, \\ a_2 &= 2E - 6\cos\delta, \\ a_3 &= -4\sin\delta, \\ a_4 &= E + 2 + \cos\delta. \end{aligned} \tag{11}$$

Namely, $a_r \equiv \text{Re}(t_1)$, $t_3 \equiv c_r + ic_i$, and $\alpha \equiv \sqrt{(\alpha_r^2 - 2a_r c_r + |c|^2)a_4}$. An example of the kink solution is displayed in Fig. 2 for $\delta = 0.1\pi$ (it is relevant to mention that this solution is different from those derived in Ref. [18] for an "asymmetric" double sine-Gordon equation).

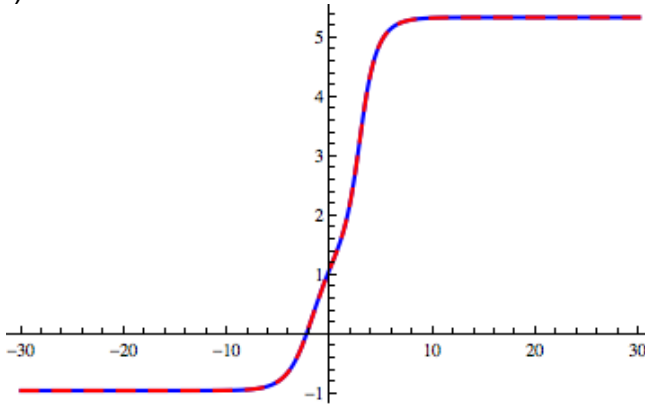
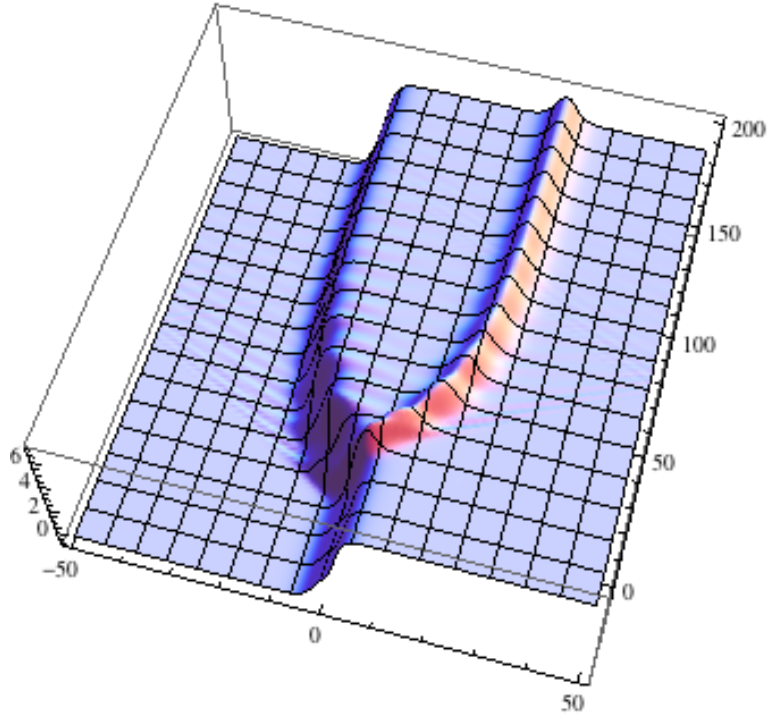


Fig. 2. (Color online). The plot of the "compound" kink connecting potential minima A and B in Fig. 1, for $\delta = 0.1\pi$. The red and blue lines depict the completely coinciding analytical solution (9) and its numerically found counterpart.

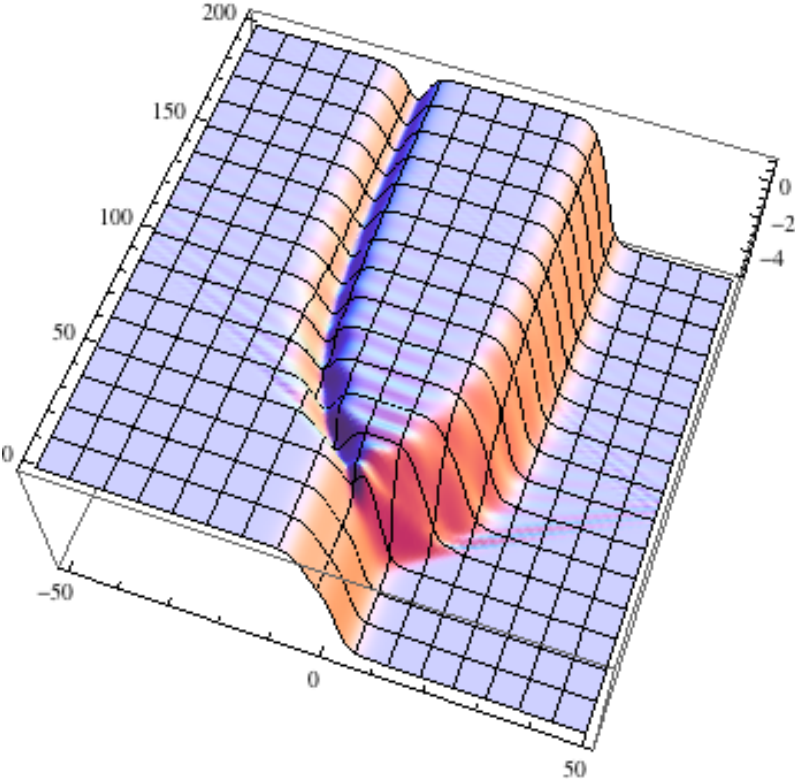
The next step is to simulate the evolution of the compound kink, within the framework of full equations (1), to test its stability. As shown in Figs. 3 and 4, the result is that the compound kink is unstable against numerical noise, eventually splitting into a pair of "simple" ones, which link pairs of points AB and CB in Fig. 1 (recall the compound kink directly connects A and B). Note that, unlike the exact solution (9) for the compound kink, explicit analytical solutions for the simple kinks are not available.

The secondary kinks produced by the breakup of the compound one separate, eventually coming to a halt due to the action of the friction terms, accounted for by coefficient α in Eqs. (1). The breakup $AB \rightarrow AC + CB$ is additionally illustrated by Fig. 5, which shows the parametric dependence between components ϕ_1 and ϕ_2 in the initial and final states of the phase fields.

Nonlinear Dynamics of Globally Coupled Sine Gordon Equations



(a)



(b)

Nonlinear Dynamics of Globally Coupled Sine Gordon Equations

Fig. 3. (Color online) The plots of $\phi_1(x,t)$ (a) and $\phi_2(x,t)$ (b) for the unstable compound kink of type AB, splitting into simple ones of types AC and CB, for $\delta = 0.1\pi$ and dissipation coefficient $\alpha = 0.04$.

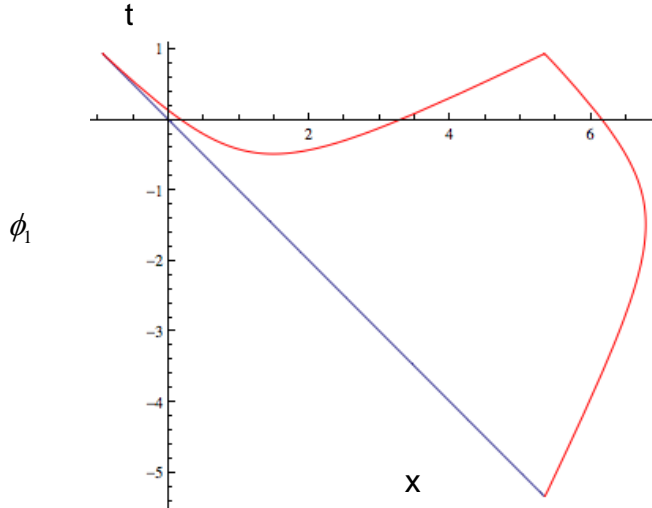


Fig. 5.(Color online). Parametric plots in the plane of (ϕ_1, ϕ_2) illustrating the breakup of the compound kink, $AB \rightarrow AC + CB$. The blue straight line corresponds to the stationary configuration at $t = 0$; the broken red line shows the same, but at $t = 200$.

The possibility for the breakup may be readily explained by the consideration of the system's energy (2). The substitution of the analytical solution (9) for the compound AB kink solution, and of numerical solutions for the simple AC and CB ones, into the integral in Eq. (2) yields the respective values of the energy (rest masses):

$m_{AB} = 25.549$, $m_{AC,CB} = 9.527$. The difference between them is a straightforward explanation to the feasibility of the splitting.

3. Bubble modes

To get the bubble solutions, which seem as solitons set on top of a constant background, featuring identical values of the phases at $x = \pm\infty$ [19], we start from the false vacuum state (shallower minimum) b in Fig. 1, and allow the test particle to travel in the anti-diagonal direction, $\phi_1 = -\phi_2$. The corresponding potential-energy profile is shown in Fig. 6.

Nonlinear Dynamics of Globally Coupled Sine Gordon Equations

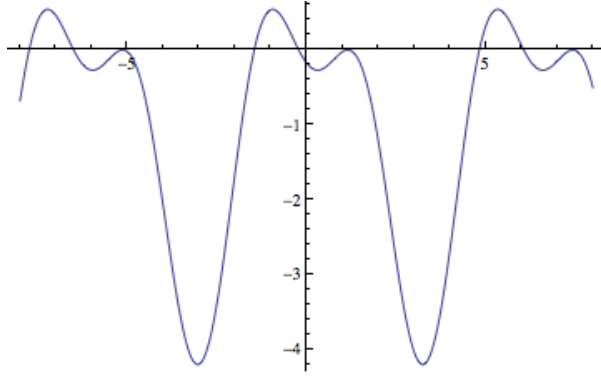
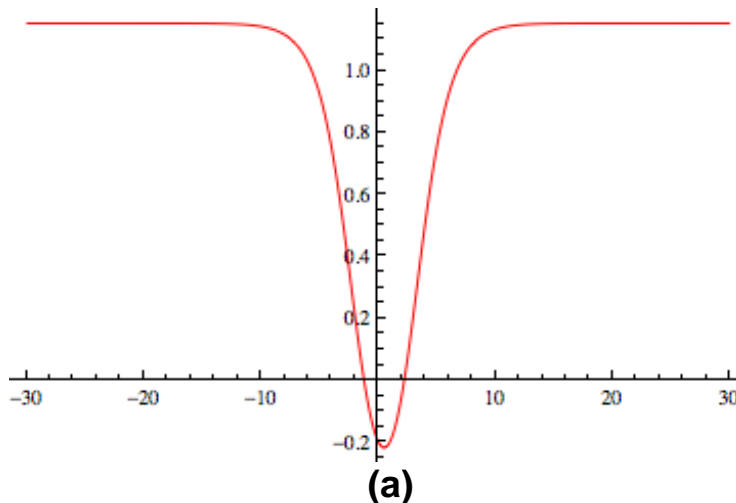


Fig. 6. (Color online) The effective potential energy, $U(\phi_1)$, corresponding to the test particle passing through point b in Fig. 1 in the direction of $\phi_1 = -\phi_2$, for $\delta = 0.1\pi$.

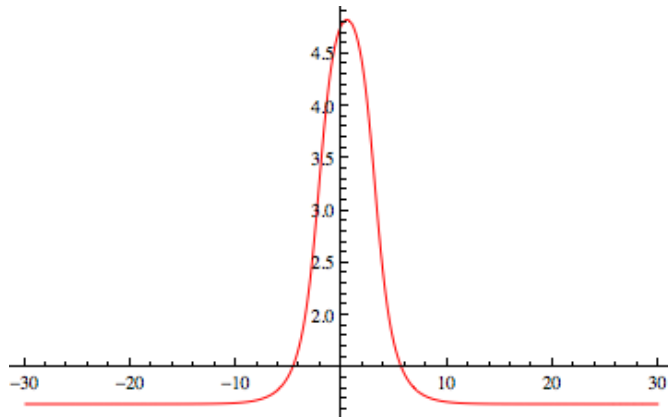
In terms of Fig. 6, a "larger" bubble corresponds to the motion from point b ($\phi_1 = 1.15$) to $\phi_1 = 4.81$ and back, while the trajectories generating another, "smaller", bubble bounces back from $\phi_1 = -0.21$. Obviously, the two bubble modes have opposite polarities (the sign of the deviation from the constant background, see also Fig. 7 below). The corresponding differential equation for $\phi_1(x)$ can be solved in an explicit form [cf. the above solution (9) for the compound kink)], yielding the following expressions for the "larger" and "smaller" bubbles:

$$\phi_{L,S}(x, \delta) = 2 \tan^{-1} \left\{ \frac{t_3(t_1 - t_2)^2 e^{2\gamma x} \mp 2\rho [t_3^2 - t_1 t_2 \pm (t_3^2 - t_3(t_1 + t_2) + t_1 t_2)] e^{\gamma x} + t_3 \rho^2}{(t_1 - t_2)^2 e^{2\gamma x} + 2\rho(t_1 + t_2 - 2t_3) e^{\gamma x} + \rho^2} \right\}, \quad (12)$$

where $\gamma(\delta) = (1/2) \left[\sqrt{(\cos \delta + E + 2)(t_3 - t_1)(t_3 - t_2)/3} \right]$, $\rho \equiv \sqrt{(t_3 - t_1)(t_3 - t_2)}$, with $t_{1,2,3}$ being the roots of polynomial (10), (11), as they were defined above. Examples of the "smaller" and "larger" bubbles with opposite polarities are displayed in Fig. 7 for $\delta = 0.1\pi$.



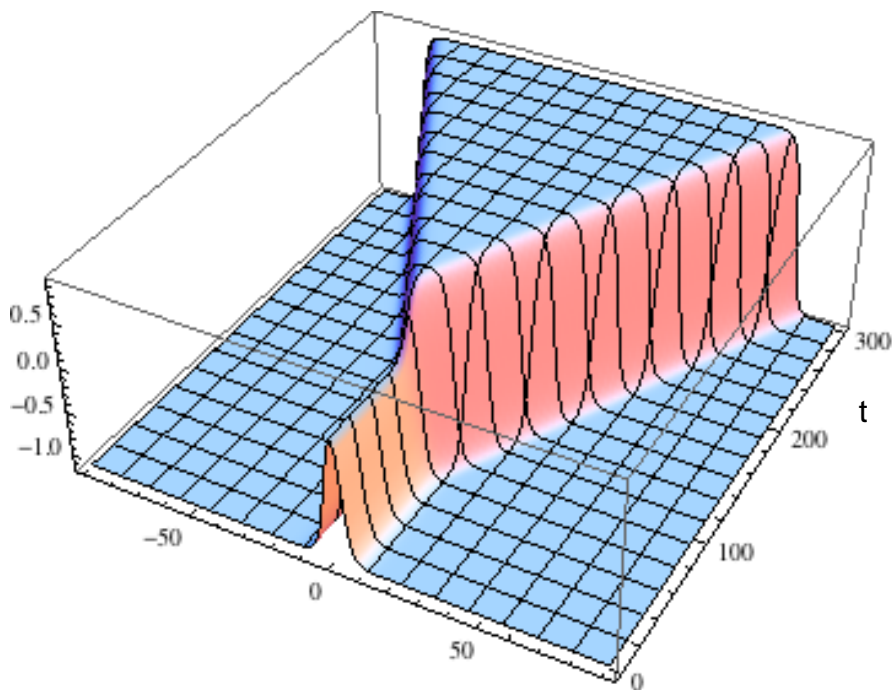
Nonlinear Dynamics of Globally Coupled Sine Gordon Equations



(b)

Fig. 7. (Color online) "Smaller" (a) and "larger" (b) bubble solutions, with the opposite polarities, found at $\delta = 0.1\pi$.

Direct simulations of Eqs. (1) demonstrate that the bubbles are metastable modes, which persist for ~ 60 time units, before the numerical noise breaks them up. The evolution of a smaller bubble is shown in Fig. for a relatively high damping parameter, $\alpha = 0.5$. The bubble's peak does not persist, relaxing back to the level corresponding to the true vacuum state. Thus, the bubble breaks up into kinks of types Ab and bA , that very rapidly reach their equilibrium velocities, which is considered in the next section, see Eq. (21).



Nonlinear Dynamics of Globally Coupled Sine Gordon Equations

Fig. 8. (Color online) The spontaneous breakup of the "smaller" bubble mode ϕ_s , see Eq. (12), at $\alpha = 0.5$ and $\delta = 0.1\pi$.

If the dissipation terms are absent, the smaller bubble breaks up into a pair of Ab and bA kinks, that move away from the origin at a velocity approaching the Swihart limit, along with excitations in a slower moving wake, see Fig. 9.

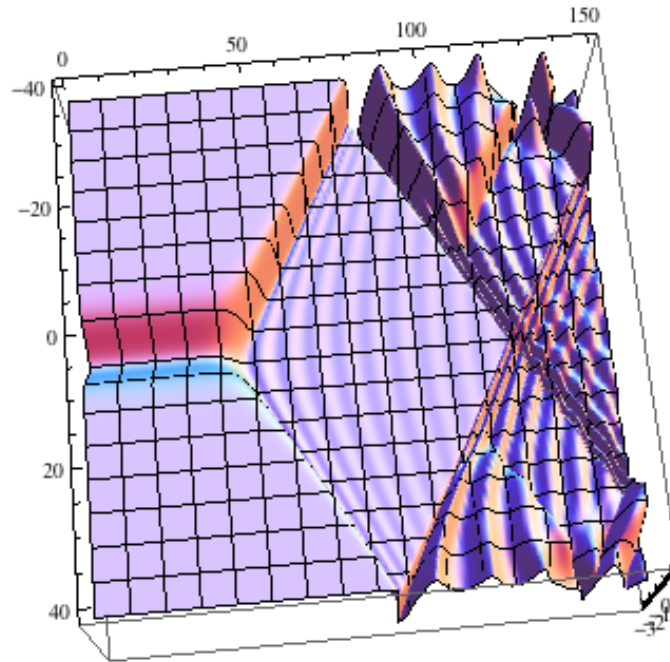


Fig. 9. (Color online) The breakup of the "smaller" bubble mode, for the same $\delta = 0.1\pi$ as in Fig. 12, but without the dissipation ($\alpha = 0$).

On the other hand, if the smaller bubble evolves with initial non-zero damping, which is then rapidly reduced to zero, the evolution proceeds differently, resulting in the formation of a persistent breather at the initial position of the bubble, see Fig. 10.

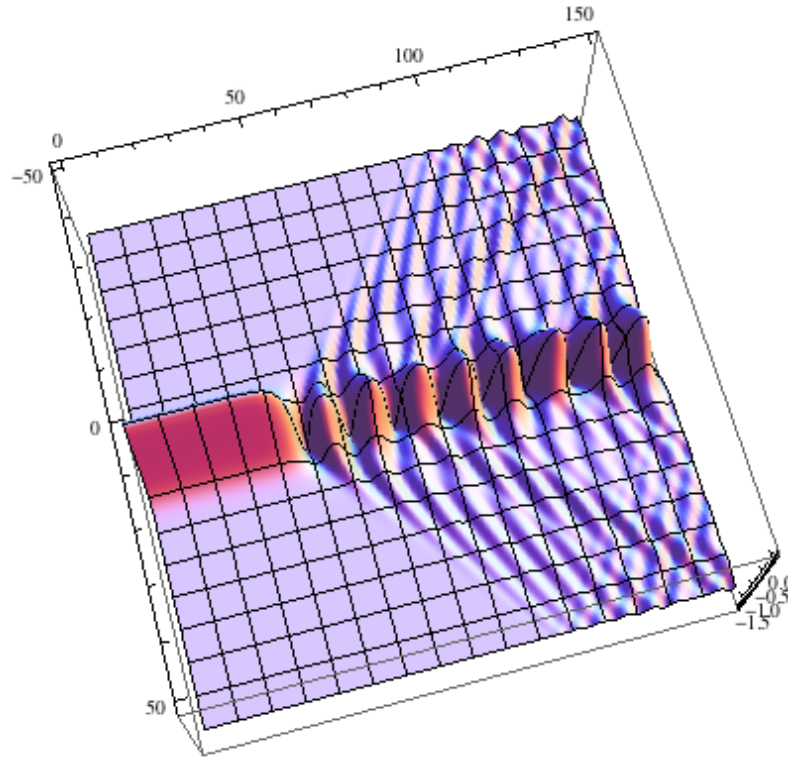


Fig. 10. (Color online) The evolution of the "small" bubble solution for $\delta = 0.1\pi$, with the damping switched off as $\alpha(t) = 0.4\exp(-t^2)$.

Finally, at values of the dissipation constant exceeding a certain critical value, $\alpha_{cr} \approx 0.6$, the bubble's peak in the corresponding *overdamped* system collapses back to the spatially uniform false-vacuum state (shallower potential minimum), inhibiting the dynamics that would lead to the emergence of the lowest potential minimum, i.e., states in which the Ab and bA kinks expand, replacing false vacuum with the true one (not shown here in detail).

The "larger" bubble mode demonstrates a behavior very similar to that of its "smaller" counterpart, with the difference that its rest mass is larger, allowing for more energy to go into the wake left after the breakup of the original bubble. When the damping coefficient is set to zero, the larger bubble also breaks up into a pair of Ab and bA kinks, that move away from the origin approaching the Swihart velocity, as shown in Fig. 11.

Nonlinear Dynamics of Globally Coupled Sine Gordon Equations

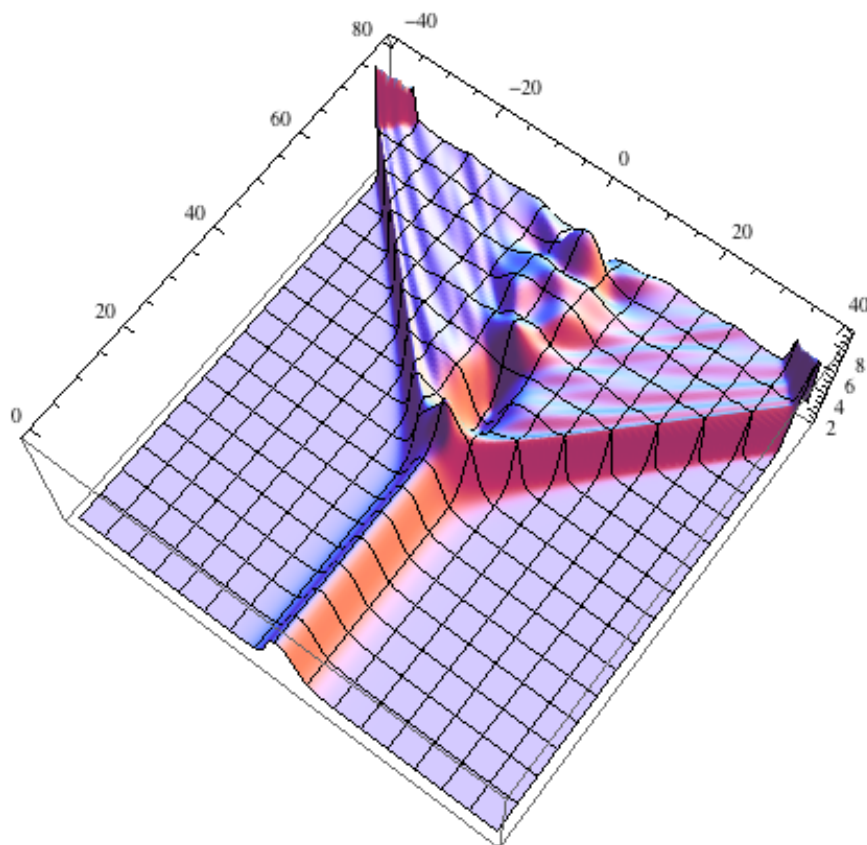
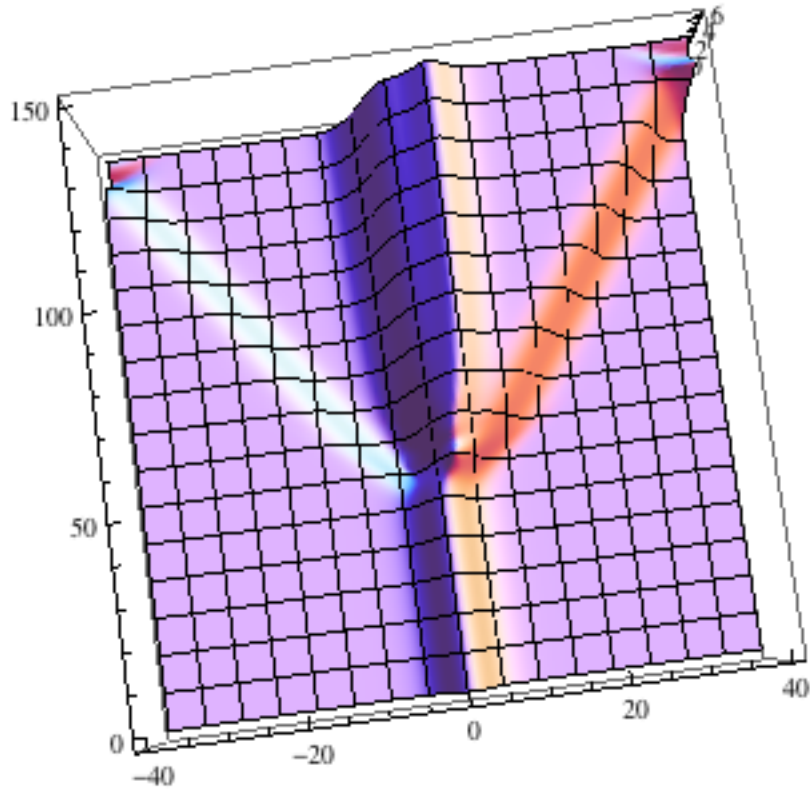


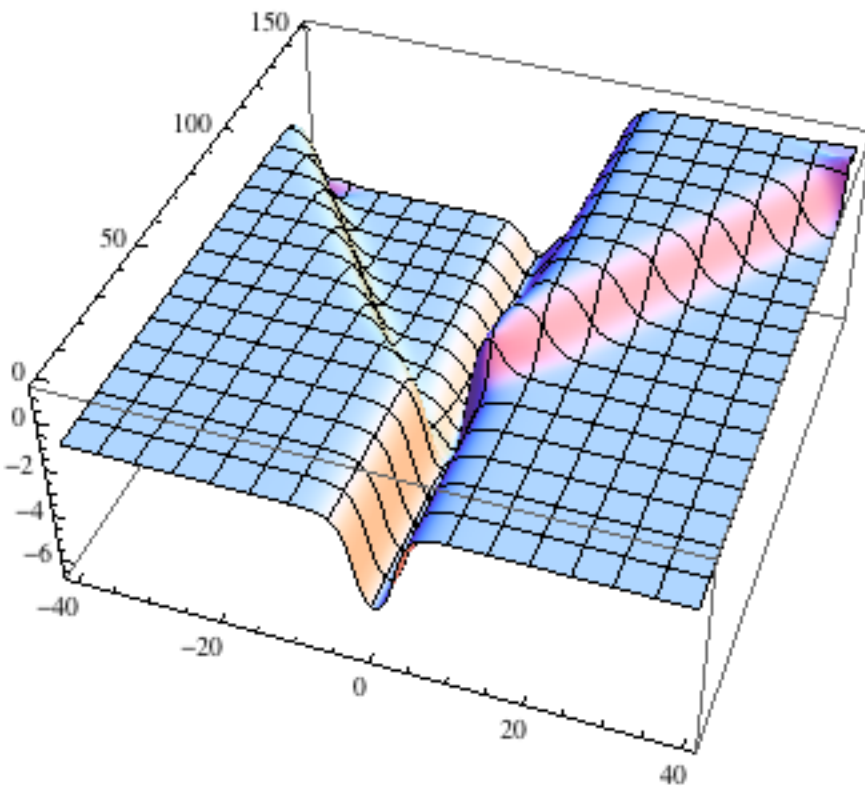
Fig. 11. (Color online). The evolution of the "larger" bubble mode at $\alpha = 0$ and $\delta = 0.1\pi$.

There is another decay scenario for the larger bubble, which is not initiated by the numerical noise alone, but may be induced by a very small relative displacement ($\sim 10^{-4}$) of the ϕ_1 and ϕ_2 components. This is shown in Fig. 12, and additionally by means of the ϕ_1 and ϕ_2 profiles at $t = 80$ in Fig. 13. In terms of Fig. 1, the final state is a path that goes from b to G along a straight line, then to C (with a bowing out of the path toward B as it does so), and then back to b along a straight line.

Nonlinear Dynamics of Globally Coupled Sine Gordon Equations



(a)



(b)

Fig. 12. (Color online) The evolution of components ϕ_1 (a) and ϕ_2 (b), corresponding to the second breakup scenario of the "larger" bubble, for $\alpha = 0$ and $\delta = 0.1\pi$.

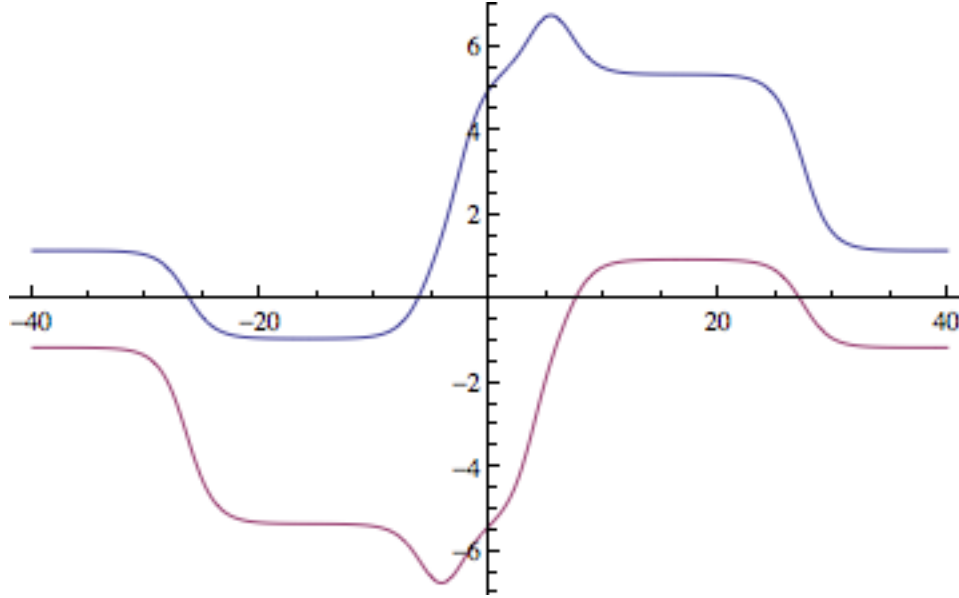


Fig. 13. Profiles of components ϕ_1 and ϕ_2 (the top and bottom lines, respectively) emerging from the second breakup scenario for the "larger" bubble, at $\alpha = 0$ and $\delta = 0.1\pi$.

4. Moving kinks (shock waves) connecting true and false vacuum states

Kinks that connect true and false vacuum states, such as corresponding to combinations fA, Ab and bC in Fig. 1, interpolate between local potential minima of different depths, hence they will be accelerated by the corresponding tilted potential [2,6]. In the presence of the dissipation, which is accounted for coefficient α in Eqs. (1), such kinks will be accelerated by the tilt until they reach an equilibrium velocity at which the tilt-induced pull is balanced by the friction force. These kinks, which may exist only in the moving form, may also be naturally considered as shock waves of the phase.

The equilibrium velocity can be predicted in an approximate analytical form by means of the momentum-balance analysis, similar to that performed by McLaughlin and Scott for kinks in the single dc-driven damped sine-Gordon equation [1,6]. To this end, the solution for the kink of the bA type (in terms of Fig. 1) may be taken as the solution available at $\delta = 0$, with a shift to account for the difference in the boundary conditions:

$$\phi_1^\delta(x, t) = \phi_1^{\delta=0}(x, t) + \delta / 3, \quad (13)$$

where the exact kink solution at zero frustration is

Nonlinear Dynamics of Globally Coupled Sine Gordon Equations

$$\phi_1^{\delta=0}(x,t) = -2 \tan^{-1} \left[\frac{\tanh\left(\frac{(x-vt)}{\sqrt{8(1-v^2)}}\right)}{\sqrt{3}} \right]. \quad (14)$$

Here v is the velocity ($v=1$ corresponds to the Swihart velocity), and

$$\phi_1^\delta(x,t) = -\phi_2^{\delta=0}(x,t). \quad (15)$$

Note that the substitution of Eqs. (14) and (15) into expression (3) for the total momentum (with $\eta=1$), and subsequent expansion up to the linear terms in the limit of $v \rightarrow 0$ makes it possible to identify the effective mass of this kink in the case of $\delta=0$ [5]:

$$m^{(bA)} = 6\sqrt{2} \left(1 - \sqrt{3}\pi/9\right) \approx 3.355. \quad (16)$$

The balance condition for momentum P implies the equilibrium between the driving force, induced by the potential tilt, and friction force, induced by the dissipative term:

$$\frac{dP}{dt} = -\alpha P_{\text{kink}} + F_{\text{dr}} = 0. \quad (17)$$

Recall that the general expression for the total momentum of system (1) is given by Eq. (3). The consideration of derivative dP/dt , in which the time differentiation is performed inside the integral expression (3), and the second time derivatives of fields $\phi_{1,2}(x,t)$ are substituted according to Eqs. (1), makes it possible to identify the term corresponding to the tilt-induced driving force. Taking into regard the boundary conditions corresponding to the kink of bA type, after somewhat lengthy but straightforward transformations the driving force is cast into the following form:

$$F_{\text{dr}}^{(bA)} = -3\sqrt{3} \sin(\delta/3). \quad (18)$$

This force is balanced by the frictional force in Eq. (17) at the equilibrium value of the momentum,

$$P_{\text{eq}}^{(bA)} = -3\sqrt{3}\alpha^{-1} \sin(\delta/3). \quad (19)$$

Finally, making use of the relativistic expression for the kink's momentum,

$$P_{\text{eq}}^{(bA)} = \frac{m^{(bA)}v}{\sqrt{1-v^2}}, \quad (20)$$

where the effective mass may be taken per Eq. (16), we obtain the final result for the equilibrium velocity of the moving kink:

$$v_{\text{eq}}^{bA} = -\frac{3\sqrt{3} \sin(\delta/3)}{\sqrt{\alpha^2 (m^{bA})^2 + 27 \sin^2(\delta/3)}} . \quad (21)$$

As a typical example of the corresponding numerical simulations of Eqs. (1), we can take the one for a moving bA kink at $\delta = \alpha = 0.1\pi$. The kink, launched at $t=0$ in the form of the explicit solution (14), (15) for $\delta = \alpha = 0$, attains the equilibrium velocity $v_{\text{eq}}^{bA} = -0.4581$, while the analytical result for the same parameters given by Eq. (21) is $v_{\text{eq}}^{bA} = -0.4579$. The simulations also demonstrate that the kink (shock wave) moving at the equilibrium velocity is completely stable.

The comparison of the shape of the numerical solution with its analytical counterpart (13)-(15), shown in Fig. 14, demonstrates a virtually ideal agreement, as well as for the equilibrium velocity.

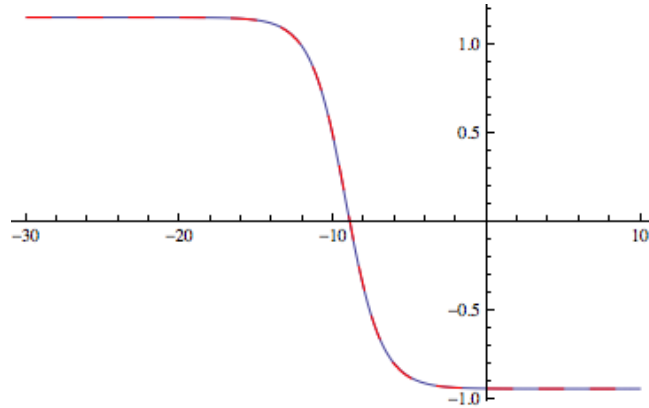


Fig. 14. (Color online). The analytical approximation for moving kink (13)-(15) (red) and its numerically found counterpart (blue), for $\delta = \alpha = 0.1\pi$.

5. Collisions between moving kinks

Collisions can occur between any two moving kinks that share a common true- or false-vacuum background. An example of the former type would be a collision between bA and Af kinks (in terms of Fig. 1), with the Ab-bC collision being an example of the latter. The tilt in the corresponding potential will act to propel the kinks so as to decrease the span of the false vacuum, simultaneously increasing the domain filled with the true vacuum.

Nonlinear Dynamics of Globally Coupled Sine Gordon Equations

This also implies that the kinks in the bA-Ab configuration would move toward the boundaries, increasing the span of true vacuum between them, while the kinks in the Ab-bA state would move on the collision course, to decrease the span of false vacuum between them. In the latter case, one may expect that the collision between the kinks will lead to their annihilation into a bound excited state, in the form of a (slowly decaying) breather. To induce the kinks to move toward one another in the former configuration, it is necessary to boost them in directions that are opposite to those of their equilibrium velocities. In that case, the kinks may rebound, simultaneously generating radiation, thus making the collision complex (if the damping is low). Examples of these two types of the collisions are presented below.

5.1. Collisions of kinks with false vacuums at domain boundaries

We first look at the simplest collision of this type, which is between the kinks of the bA and Ab types. There are some practical constraints in carrying out the corresponding numerical experiments, the first of which is that the two kinks must be well separated initially. Further, setting the two kinks far from each other initially means that they must be launched with sufficiently large velocities, so that they may collide before the tilt in the potential will reverse their trajectories, as mentioned above.

Another constraint for numerical simulations stems from the boundary conditions at edges of the integration domain, $x = \pm L$. Boundary conditions of two types have been employed in simulations of the collisions: the no-radiation constraint,

$$\begin{aligned} [\partial\phi_i/\partial x + \partial\phi_i/\partial t] &= 0, \quad x = -L, \\ [\partial\phi_i/\partial x - \partial\phi_i/\partial t] &= 0, \quad x = +L, \end{aligned} \tag{22}$$

and the zero-magnetic-field condition,

$$[\partial\phi_i/\partial x] = 0 \text{ at } x = \pm L. \tag{23}$$

Since the no-radiation condition can still allow reflections of slowly moving disturbances, we have used, in most cases, a combination of the zero-magnetic-field condition with an absorber (a stripe with an artificially high damping coefficient, attached to each boundary).

The example of the collision shown below is for the bA-Ab configuration with a small damping coefficient, $\alpha = 0.02$, and the same value of the frustration as used above, *viz.* $\delta = 0.1\pi$. The initial field was taken as the joined pair of exact kinks for $\alpha = \delta = 0$, with the separation between them $2x_0 = 30$ and velocities $v = \pm 0.99$.

Nonlinear Dynamics of Globally Coupled Sine Gordon Equations

$$\begin{aligned} \phi_1(x, t = 0) = & \left\{ 2 \tan^{-1} \left[\frac{\tanh((x - x_0) / \sqrt{8})}{\sqrt{3(1 - v^2)}} \right] + \frac{\delta}{3} \right\} \theta(x) \\ & - \left\{ 2 \tan^{-1} \left[\frac{\tanh((x - x_0) / \sqrt{8})}{\sqrt{3(1 - v^2)}} \right] + \frac{\delta}{3} \right\} \theta(-x), \end{aligned} \quad (24)$$

as shown in Fig. 15. a typical result of the collision is displayed in Fig. 16.

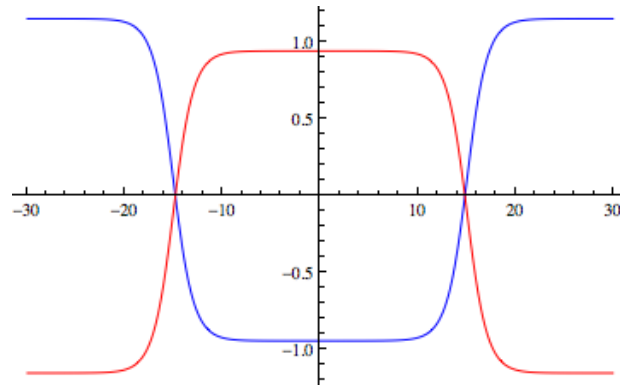


Fig. 15. (Color online) The initial bA-Ab pair of boosted kinks, prepared for the collision: the ϕ_1 (blue, with the minimum at $x = 0$) and ϕ_2 (red, with a maximum at $x = 0$) components.

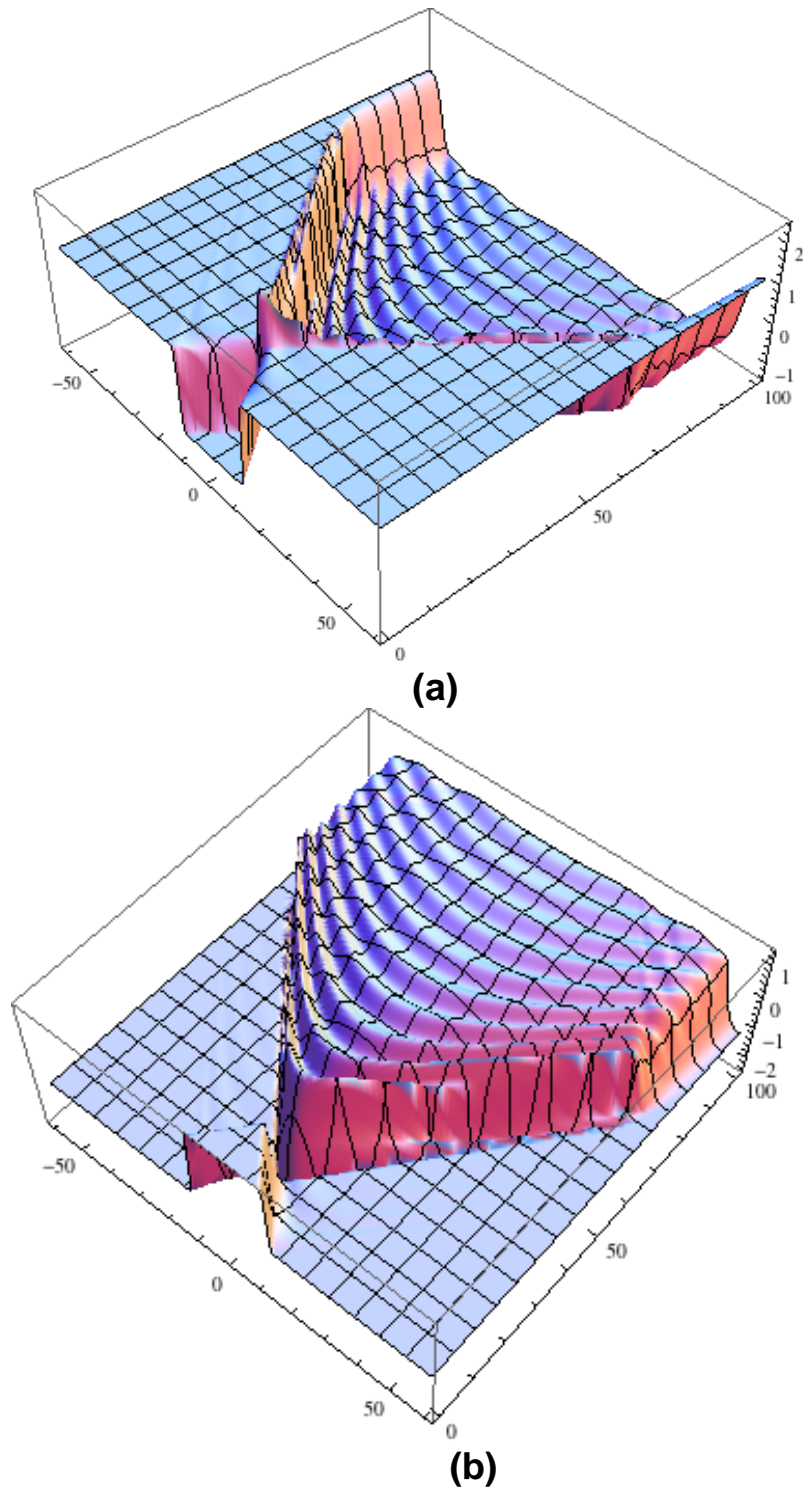


Fig. 16. (Color online) (a) and (b): Plots of the evolution of fields $\phi_{1,2}(x,t)$ in the course of the collision of the bA-Ab type, with initial inward velocities, $v = \pm 0.99$ and damping constant $\alpha = 0.02$.

In the case of the bA-Af collision, the picture is essentially the same as in Fig. 16, with an obvious difference that component $\phi_2(x,t)$ in the Af kink makes an extra 2π jump.

When the damping coefficient is set to zero, $\alpha = 0$, Fig. 17 shows that a long-lived breather can be excited at the origin by the annihilation of the colliding bA-Af pair (which is not the case for the bA-Ab collision). This outcome is possible because the difference between the b and f states in Fig. 1 is $\Delta\phi_2 = 2\pi$.

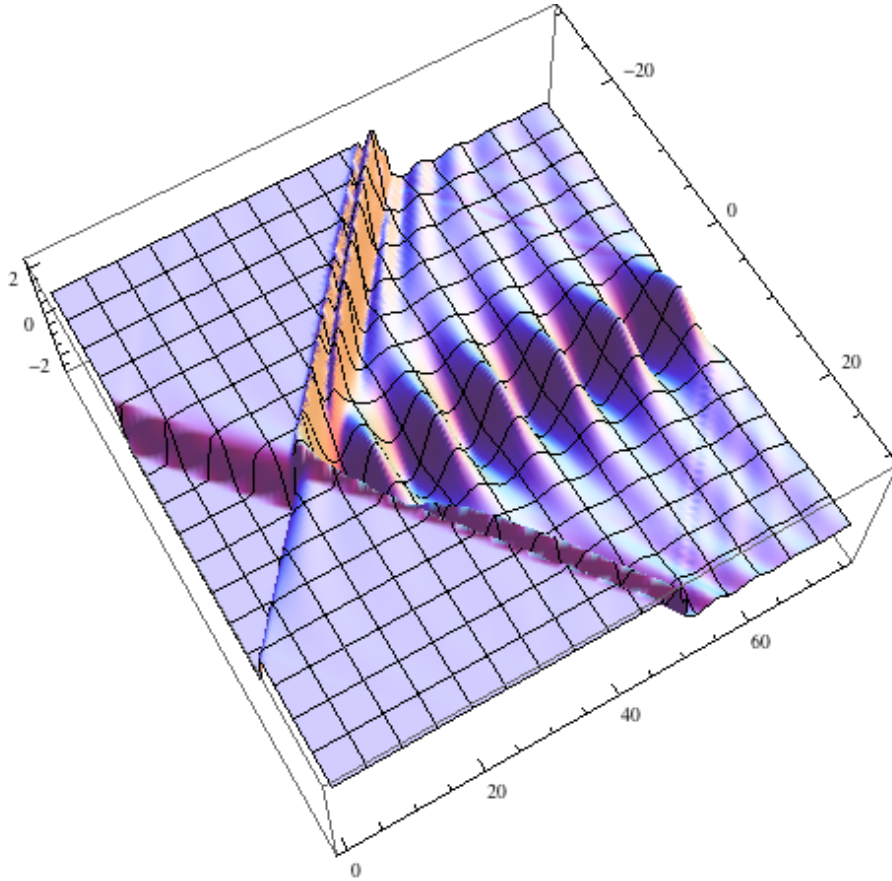


Fig. 17. (Color online) The plot of $\phi_1(x,t)$ illustrating the formation of the breather following the bA-Af collision with initial inward velocities $v = \pm 0.99$ and zero damping, $\alpha = 0$.

5.2 . Collisions between traveling kinks with true vacua at boundaries

Finally, we consider the collision of the second type (as defined above), when the two kinks are supported by true vacuum states at the spatial boundaries, sharing a false vacuum state in the region between them. An example is the collision between Ab and bC kinks, that are launched toward the origin at $t = 0$ and at the equilibrium velocities, see Eq. (21), from well-separated locations, as shown below in Fig. 18.

Nonlinear Dynamics of Globally Coupled Sine Gordon Equations

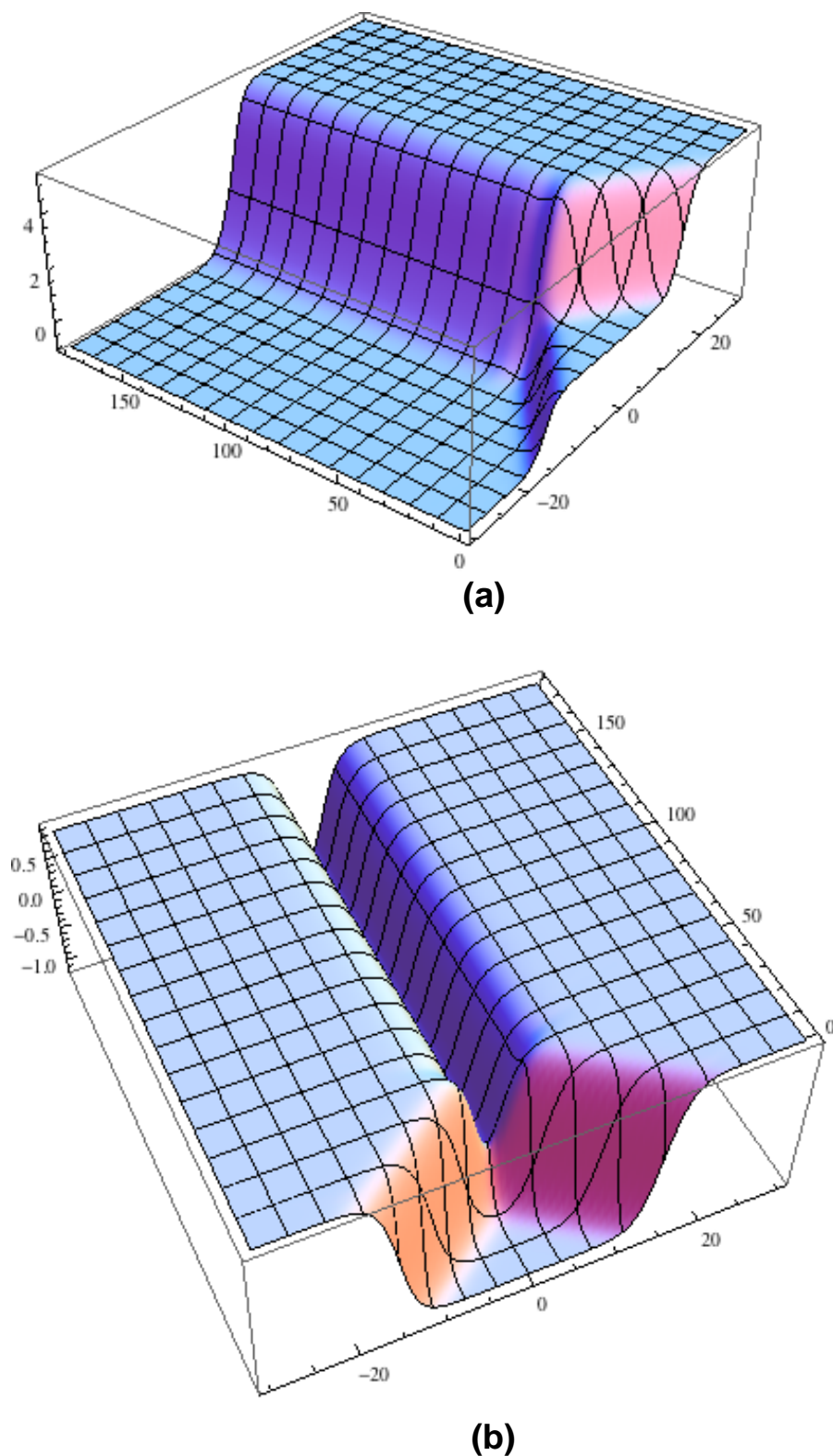


Fig 18. (Color online) (a) and (b): Plots of $\phi_1(x,t)$ and $\phi_2(x,t)$ illustrating in the collision of the Ab and bC kinks for $\alpha = \delta = 0.1\pi$, initially moving at the corresponding equilibrium velocities [see Eq. (21)], $v = \pm 0.4581$.

As seen, this collision leads (quite naturally) to the fusion of the colliding kinks into a quiescent one of the AC type. For other pairs of moving kinks with the shared false vacuum initially located between them, the outcome is similar, also featuring the fusion into an immobile kink interpolating between two true vacuums.

6. Conclusions

This paper reports results of the systematic analysis of the dynamics of fluxons (kinks) in the fundamental prismatic configuration formed by three bulk superconductors, which creates a set of three parallel long Josephson junctions at interfaces between them. The setting is described by a system of three coupled sine-Gordon equations for the phases corresponding to each junction. In fact, the condition for the external magnetic flux trapped by the system reduces the model to two equations. The equations include the dissipative terms, and are controlled by the frustration parameter, that measures the deviation of the external flux from half a quantum. Analyzing the corresponding potential profile, we have identified different types of topological kink solitons, which correspond to fluxons, in terms of the coupled junctions. Nontopological "bubble" modes have been found too. Some solutions, including those for "compound" kinks and for two types of the bubbles, were obtained in an analytical form. Numerical simulations demonstrate that the compound kinks are unstable against breaking up into pairs of simple kinks. Bubbles are metastable objects, that eventually break up into kink-antikink pairs. The system also gives rise to kinks which connect different potential minima, hence they are pulled by the tilt of the potential. Using the momentum-balance method, we have derived the equilibrium velocity at which such driven kinks should move, and verified the prediction by simulations. Finally, collisions between the moving kinks were studied by means of direct simulations, which demonstrate that the collisions are always strongly inelastic.

References

1. D. W. McLaughlin and A. C. Scott, Phys. Rev. A **18**, 1652 (1978).
2. B. A. Malomed, Phys. Lett. A **136**, 395 (1989).
3. G. S. Mkrtchyan and V. V. Shmidt, Solid State Commun. **30**, 791 (1979); B. Dueholm, O. A. Leving, J. Mygind, N. F. Pedersen, O. H. Soerensen, and M. Cirillo, Phys. Rev. Lett. **46**, 1299 (1981); E. Joergensen, V. P. Koshelets, R. Monaco, J. Mygind, M. R. Samuelsen, and M. Salerno, *ibid.* **49**, 1093 (1982); M. Salerno, M. R. Samuelsen, G. Filatrella, S. Pagano, and R. D. Parmentier, Phys. Rev. B **41**, 6641 (1990); J. G. Caputo, N. Flytzanis, and M. Devorte, *ibid.* **50**, 6471 (1994); R. G. Mints and I. B. Snapiro, *ibid.* **52**, 9691 (1995); M. Cirillo, N. Grønbech-Jensen, M. R. Samuelsen, M. Salerno, and G. V. Rinati, *ibid.* **58**, 12377 (1998).
4. Yu. S. Kivshar and B. A. Malomed, Phys. Rev. B **37**, 9325 (1988); A. V. Ustinov, H. Kohlstedt, M. Cirillo, N. F. Pedersen, G. Hallmanns, and C. Heiden, *ibid.* B **48**, 10614 (1993); N. Grønbech-Jensen and M. R. Samuelsen, *ibid.* **48**, 16160 (1993); and J. A. Blackburn, Phys. Rev. Lett. **70**, 1251 (1993); N. Grønbech-

Nonlinear Dynamics of Globally Coupled Sine Gordon Equations

- Jensen, D. Cai, A. R. Bishop, A. W. G. Lau, and P. S. Lomdahl, *Phys. Rev. B* **50**, 6352 (1994); Z. Hermon, E. Ben-Jacob, and G. Schön, *ibid.* **B 54**, 1234 (1996); S. Watanabe, H. S. J. van der Zant, S. H. Strogatz, and T. P. Orlando, *Physica D* **97**, 429 (1996); G. Hechtfisher, R. Kleiner, K. Schlenga, W. Walkenhorst, P. Muller, and H. L. Johnson, *Phys. Rev. B* **55**, 14638 (1997); E. Goldobin, A. Wallraff, N. Thyssen, and A. V. Ustinov, *ibid.* **57**, 130 (1998); V. M. Krasnov, V. A. Oboznov, V. V. Ryazanov, N. Mros, A. Yurgens, and D. Winkler, *ibid.* **61**, 766 (2000); E. Goldobin, B. A. Malomed, and A. V. Ustinov, *ibid.* **62**, 1414 (2000); R. Kleiner, T. Gaber, and G. Hechtfisher, *ibid.* **62**, 4086 (2000); M. Machida, T. Koyama, A. Tanaka, and M. Tachiki, *Physica C* **330**, 85 (2000); E. Goldobin, A. Wallraff, and A. V. Ustinov, *J. Low Temp. Phys.* **119**, 589 (2000); C. Gorria, P. L. Christiansen, Y. B. Gaididei, V. Muto, N. F. Pedersen, and M. P. Soerensen, *Phys. Rev. B* **68**, 035415 (2003).
5. S. P. Yukon and N. H. Lin, *IEEE Trans. Mag.* **27**, 2736 (1991).
 6. Yu. S. Kivshar and B. A. Malomed, *Rev. Mod. Phys.* **61**, 763 (1989).
 7. N. F. Pedersen, *Physica D* **68**, 27 (1993); N. F. Pedersen and A. V. Ustinov, *Supercond. Science and Technology* **8**, 389 (1995); A. V. Ustinov, *Physica D* **123**, 315 (1998).
 8. L. M. Floria and J. J. Mazo, *Adv. Phys.* **45**, 505 (1996); O. M. Braun and Yu. S. Kivshar, *Phys. Rep.* **306**, 1 (1998).
 9. S. Savel'ev, V. A. Yampol'skii, A. L. Rakhmanov, and F. Nori, *Rep. Progr. Phys.* **73**, 026501 (2010).
 10. J. Yang and S. P. Yukon, unpublished [AFRL Final Report (F33601-02-F-A581-P00010)].
 11. T. Kapitula, P. G. Kevrekidis, and Z. G. Chen, *SIAM J. Appl. Dyn. Systems* **5**, 598 (2006); K. Huybrechts, G. Morthier, and B. Maes, *J. Opt. Soc. Am. B* **27**, 708 (2010).
 12. V. S. Shchesnovich and D. S. Mogilevtsev, *Phys. Rev. A* **82**, 043621 (2010).
 13. B. Liu, L.-B. Fu, S.-P. Yang, and J. Liu, *Phys. Rev. A* **75**, 033601 (2007); T. F. Viscondi, K. Furuya, and M. C. de Oliveira, *EPL* **90**, 10014 (2010).
 14. T. Lahaye, T. Pfau, and L. Santos, *Phys. Rev. Lett.* **104**, 170404 (2010).
 15. A. Gubeskys and B. A. Malomed, *Eur. Phys. J. D* **28**, 283 (2004).
 16. Z. Yan, K. W. Chow, and B. A. Malomed, *Chaos, Solitons & Fractals* **42**, 3013 (2009).
 17. A. Sigler, B. A. Malomed, and D.V. Skryabin, *Phys. Rev. E* **74**, 066604 (2006).
 18. N.-H. Kuo, S. Sarkar, and C. D. Hu, arXiv:0909.1872 (2009).
 19. I. V. Barashenkov and E. Y. Panova, *Physica D* **69**, 114 (1993); I. V. Barashenkov, *Phys. Rev. Lett.* **77**, 1193 (1996).